INFECTION AND IMMUNITY, July 2011, p. 2586–2596 Vol. 79, No. 7
0019-9567/11/$12.00 doi:10.1128/IAI.00920-10

Increased Disease Severity of Parasite-Infected TLR2$^{-/-}$ Mice Is Correlated with Decreased Central Nervous System Inflammation and Reduced Numbers of Cells with Alternatively Activated Macrophage Phenotypes in a Murine Model of Neurocysticercosis$^{\nabla}$

Uma Mahesh Gundra,[1]† Bibhuti B. Mishra,[1]† Kondi Wong,[2] and Judy M. Teale[1]*

Department of Biology, South Texas Center for Emerging Infectious Diseases, The University of Texas at San Antonio, One UTSA Circle, San Antonio, Texas 78249-1644,[1] and Department of Pathology, Tampa General Hospital, One Tampa Circle, Tampa, Florida 33606[2]

Received 23 August 2010/Returned for modification 20 September 2010/Accepted 1 April 2011

In a murine model for neurocysticercosis (NCC), intracranial inoculation of the helminth parasite *Mesocestoides corti* induces multiple Toll-like receptors (TLRs), among which TLR2 is upregulated first and to a relatively high extent. Here, we report that TLR2$^{-/-}$ mice displayed significantly increased susceptibility to parasite infection accompanied by increased numbers of parasites in the brain parenchyma compared to infection in wild-type (WT) mice. This coincided with an increased display of microglial nodule formations and greater neuropathology than in the WT. Parasite-infected TLR2$^{-/-}$ brains exhibited a scarcity of lymphocytic cuffing and displayed reduced numbers of infiltrating leukocytes. Fluorescence-activated cell sorter (FACS) analyses revealed significantly lower numbers of CD11b^{+} myeloid cells, γδ T cells, αβ T cells, and B cells in the brains of parasite-infected TLR2$^{-/-}$ mice. This correlated with significantly reduced levels of inflammatory mediators, including tumor necrosis factor alpha (TNF-α), gamma interferon (IFN-γ), CCL2, CCL3, and interleukin-6 (IL-6) in the central nervous system (CNS) of TLR2$^{-/-}$ mice. As TLR2 has been implicated in immune regulation of helminth infections and as alternatively activated macrophages (AAMs) are thought to play a profound regulatory role in such infections, induction of AAMs in infected TLR2$^{-/-}$ mice was compared with that in WT mice. Parasite-infected WT brains showed larger numbers of macrophages/microglia (CD11b^{+} cells) expressing AAM-associated molecules such as YM1, Fizz1 (found in inflammatory zone-1 antigen), and arginase 1 than TLR2$^{-/-}$ brains, consistent with a protective role of AAMs during infection. Importantly, these results demonstrate that TLR2-associated responses modulate the disease severity of murine NCC.

Neurocysticercosis (NCC) is a disease of the central nervous system (CNS) caused by the metacestode of the tapeworm *Taenia solium* (*T. solium*). This is the most common parasitic disease of the CNS and is a major cause of acquired epilepsy in adults (32, 57, 63). In humans, *T. solium* exhibits a biphasic life cycle in which the infection manifests in a long asymptomatic phase during which the parasite stays dormant in the form of a cyst with no detectable inflammatory response surrounding the parasite. A symptomatic episode may follow this asymptomatic phase which rapidly leads to convolutions, cranial hypertension, and cognitive disorders (64, 65). The type and severity of symptoms depend on size, number, and anatomical location of the parasites in addition to the intensity of the immune response. The immune response in the CNS of symptomatic patients consists of an overt Th1 phenotype (53) or a mixed Th1, Th2, and Th3 phenotype, depending upon the absence or presence of granuloma formation (52). However, the appropriate immune responses required and effector mechanisms involved in restricting parasite growth and controlling disease severity in NCC are still not clear.

Due to the absence of a classically defined lymphatic system, innate immune responses appear to be key elements in promoting immune responses in the CNS. Recent studies have demonstrated the critical role played by the Toll-like receptor (TLR) family of proteins in host innate immunity (24). Once engaged, most TLRs signal through a common pathway involving MyD88 (55) that leads to the downstream activation of the NF-κB and mitogen-activated protein kinase (MAPK) pathways inducing a Th1 proinflammatory response (35). Nevertheless, emerging evidence indicates that TLRs can elicit anti-inflammatory regulatory T (Treg) cells and Th2-associated responses as well as the induction of alternatively activated macrophages (AAMs) (15, 16, 49, 51). This suggests a larger role for TLRs in immune regulatory mechanisms involved in various clinical settings. However, the functions of TLRs in nervous system parasitic diseases, including NCC, are only beginning to emerge (17, 39, 56, 66, 67).

In a murine model for NCC, we have previously shown that intracranial (i.c.) infection of mice with *Mesocestoides corti* metacestodes results in differential expression of TLRs (36, 40). Among all the TLRs, TLR2 expression was the first to be induced and was substantially upregulated during infection. In the present study the susceptibility and immunopathology of TLR2$^{-/-}$ and wild-type (WT) NCC mice were compared. The contribution of TLR2 signaling to CNS inflammation was assessed by measuring the proinflammatory cytokine responses

* Corresponding author. Mailing address: Department of Biology, The University of Texas at San Antonio, One UTSA Circle, San Antonio, TX 78249-1644. Phone: (210) 458-7024. Fax: (210) 458-7025. E-mail: judy.teale@utsa.edu.

† U.M.G. and B.B.M. contributed equally to the work.

$^{\nabla}$ Published ahead of print on 11 April 2011.

in the CNS and the infiltration of various immune cells into the brain of TLR2$^{-/-}$ and WT mice. Additionally, the accumulation/induction of AAMs that are known to function in tissue restoration was measured. The results indicate that TLR2-mediated responses help to mitigate not only CNS pathology but also mortality due to infection in murine NCC.

MATERIALS AND METHODS

Mice. Female mice (5 weeks old) were used in this study. TLR2$^{-/-}$ and MyD88$^{-/-}$ mice on the C57BL/6 background (originally from S. Akira, Osaka University, Osaka, Japan) were kindly provided by Michael Berton (Department of Microbiology and Immunology, University of Texas Health Science Center, San Antonio, TX). C57BL/6 mice were obtained from the National Cancer Institute animal program (Bethesda, MD) and used as WT controls. WT and TLR2$^{-/-}$ mice were bred in the University of Texas—San Antonio (UTSA) animal facility. Female BALB/c mice, used in this study for parasite maintenance, were obtained from the National Cancer Institute animal program (Bethesda, MD). Interleukin-4 receptor alpha-deficient (IL-4R$\alpha^{-/-}$) mice on the BALB/c background were obtained from the Jackson Laboratory and were used as controls. All animal experiments were conducted under the guidelines of the IACUC, University of Texas System, the U.S. Department of Agriculture, and the National Institutes of Health.

Antibodies. Phycoerythrin (PE)-conjugated antibodies purchased from BD PharMingen (San Diego, CA) include the following: GL3 (pan-anti-γδ), H57-597 (pan-anti-αβ), M1/70 (anti-Mac1), 1D3 (anti-CD19), R35-95 [anti-rat IgG2a(κ)], B81-3 [anti-hamster IgG2(κ)], and HA4/8 [anti-hamster IgG2(λ)]. Purified 2.4G2 (anti-CD16/32), anti-mouse IL-6, anti-mouse IL-4 (BVD4-1D11), anti-mouse glial fibrillary acidic protein (GFAP), and biotinylated anti-mouse CD11b were also purchased from BD PharMingen. Anti-mouse GFAP was conjugated to Alexa Fluor 488 (Molecular Probes, Eugene, OR) according to the manufacturer's instructions. IL-13 in the brain was detected by using purified anti-mouse IL-13 (Santa Cruz Biotechnology) or PE-conjugated anti-IL-13 (clone eBio13A; eBiosciences); AAMs in the brain were detected by using purified anti-mouse YM1 (ECF-L) (R&D Systems), anti-mouse Fizz1 (RELMα) (Abcam, Cambridge, MA), or anti-mouse arginase 1 (ARG-1) (Santa Cruz Biotechnology, CA). For indirect immunofluorescence (IF) staining, appropriate fluorescently conjugated secondary antibodies (Jackson Immuno Research Laboratories, West Grove, PA) were used. Biotinylated primary antibodies were detected using Alexa Fluor 488-labeled streptavidin (Molecular Probes).

Murine model of neurocysticercosis. In this study we used a mouse model of NCC developed in our laboratory (11, 12). *M. corti* metacestodes were maintained by serial intraperitoneal (i.p.) inoculation of 8- to 12-week-old female BALB/c mice. Metacestodes were aseptically harvested, and murine NCC was induced by i.c. injection (just below the dura) of 50 μl of Hanks balanced salt solution (HBSS) containing approximately 40 parasites into 5-week-old mice under short-term anesthesia. The anesthesia was a 50-μl mixture of ketamine HCl and xylazine (30 mg/ml ketamine and 4 mg/ml xylazine) in phosphate-buffered saline (PBS) that was injected intramuscularly, as described previously (11). Mock-infected control mice were similarly injected with 50 μl of sterile HBSS alone. At indicated times postinoculation, anesthetized animals were perfused through the left ventricle with 10 ml of cold PBS, and brains were harvested to analyze parasite burden and various immune parameters.

Histology and immunofluorescence staining. The brains were immediately removed from perfused animals, embedded in OCT resin (optimal cutting temperature), and snap frozen. Serial horizontal cryosections, 10 μm in thickness, were placed on silane prep slides (Sigma-Aldrich, St. Louis, MO). One in every five slides was fixed in formalin for 12 min at room temperature (RT) and stained with hematoxylin and eosin (H&E), as described previously (39). The remainder of the slides were air dried overnight and fixed in fresh acetone for 20 s at RT. Acetone-fixed sections were wrapped in aluminum foil and stored at −80°C or processed immediately for *in situ* IF microscopy analysis as previously described (4, 5, 10, 40).

Luxol blue staining. Luxol blue staining on brain sections from mock- and parasite-infected WT and TLR2$^{-/-}$ mice was performed as described previously (29). Briefly, dissected brains were stored in 10% buffered formalin overnight for histological processing. Brains were dehydrated through graded alcohol, cleared with xylene, and embedded in paraffin. Transverse sections were cut at 5-μm thicknesses and were placed on silane prep slides. Sections were deparaffinized in xylene for 5 min, rehydrated in 95% ethanol for 5 min at RT, and stained with preheated Luxol fast blue (LFB; Polysciences, Warrington, PA) at 60°C overnight. Slides were washed for 1 min in 95% ethanol in deionized water and incubated in 0.05% lithium carbonate (Sigma Aldrich, St. Louis, MO) followed by 70% ethanol for 3 to 4 min. The sections were then rinsed in deionized water for 30 s and counterstained with cresyl etch violet (Sigma Aldrich, St. Louis, MO), dehydrated through a 95% and 100% alcohol series for 5 min each, cleared in xylene, and cover slipped with synthetic resin.

Brain mononuclear cell isolation and FACS analysis. Leukocytes from mouse brains were isolated (26) and processed for IF staining of cell surface antigens for flow cytometric analysis (fluorescence-activated cell sorting [FACS] analysis) as described previously (39). Single-cell suspensions of harvested leukocytes from parasite-infected brains of WT and TLR2$^{-/-}$ mice were prepared at 2×10^7 cells/ml in staining buffer (10% FCS in PBS) and preincubated with 1 μg of the 2.4G2 antibody for 5 to 10 min on ice prior to staining. Fifty microliters of cell suspension (equal to 10^6 cells) was dispensed into each tube along with a previously determined optimal concentration of cell surface-specific antibodies in 50 μl of staining buffer. Each test tube was mixed gently and incubated for 30 min in the dark in an ice bath. Cells were stained with fluorochrome-labeled antibodies of the appropriate isotype control for nonspecific binding. Cells stained in the absence of primary antibodies served as negative controls. After the incubation period, cells were washed by adding 2 ml of staining buffer, followed by centrifugation for 7 min (at 300 to 400 × g) at 4°C. The washing was repeated two more times for a total of three washes. Cell pellets were suspended in 500 μl of staining buffer and analyzed on a BD LSR II flow cytometer (BD Biosciences).

ELISA. Brain homogenates were centrifuged at 2,000 × *g* for 15 min to clear cellular debris, and the supernatants were frozen immediately at −80°C. Levels of tumor necrosis factor alpha (TNF-α), gamma interferon (IFN-γ), and CCL2 in brain homogenates were determined by using BD OptEIA enzyme-linked immunosorbent assay (ELISA) kits (BD Biosciences). Dilutions of TNF-α, IFN-γ, and CCL2 standards of known concentrations as well as dilutions of brain homogenate supernatants were added to 96-well plates precoated with anticytokine antibodies (Abs) and preblocked with PBS containing 10% fetal bovine serum (FBS). Samples were incubated at RT for 2 h. After samples were washed, biotinylated anticytokine Abs were diluted in PBS containing 10% FBS and added for 1 h at RT. After samples were washed, horseradish peroxidase (HRP)-conjugated streptavidin A in PBS containing 10% FBS was added for 30 min at RT. After final washes, the HRP substrate TMB (3,3′,5,5′-tetramethylbenzidine) was added, and the optical density of the color reaction was measured at 450 nm. Concentrations of cytokine in the culture supernatant were calculated using standard curves as references.

Quantification of ARG-1 and Fizz1 protein expression. Sections of brains from mock-infected and NCC mice were stained with specific anti-ARG-1 and anti-Fizz1 antibodies, followed by labeled secondary antibodies to quantify the differences in protein levels. Brain sections were additionally stained with antibodies against CD11b to assess localization of ARG-1 and Fizz1 with infiltrating macrophages/microglia. Protein expression levels of these molecules were determined by capturing images at a magnification of ×20 from areas containing AAMs in the brain of mock-infected and NCC animals. Images were captured using identical camera settings so that the number and intensity of pixels would reflect differences in protein expression (36, 39). The area (number of pixels) and fluorescent intensity (average intensity of pixels) of the staining from 10 images were measured. This was done using the imaging software IPLab, version 4.0 (BD Biosciences Bioimaging, Rockville MD). The relative expression of Fizz1 and ARG-1 was calculated by multiplying the number of pixels (area) by the average intensity of pixels.

Statistical analysis. We used a Student's *t* test for comparison of means of different groups (Sigma PLOT, version 8.0; Systat Software, San Jose, CA). A P value of <0.05 was considered to be statistically significant. Statistical differences for mortality of parasite-infected NCC mice were analyzed using Kaplan-Meir survival analysis.

RESULTS

TLR2$^{-/-}$ mice are more susceptible to parasite infection in murine NCC. We demonstrated previously that CNS infection with *M. corti* results in the dynamic upregulation of TLR2 in nervous tissue cells early during infection (40). To investigate whether TLR2 influences immunity to this infection, disease severity was compared between WT and TLR2$^{-/-}$ mice infected i.c. with *M. corti*. As reported previously (11, 12), infected WT mice displayed typical neurological signs, including abnormal vestibular function, tilted head, cerebral abnormali-

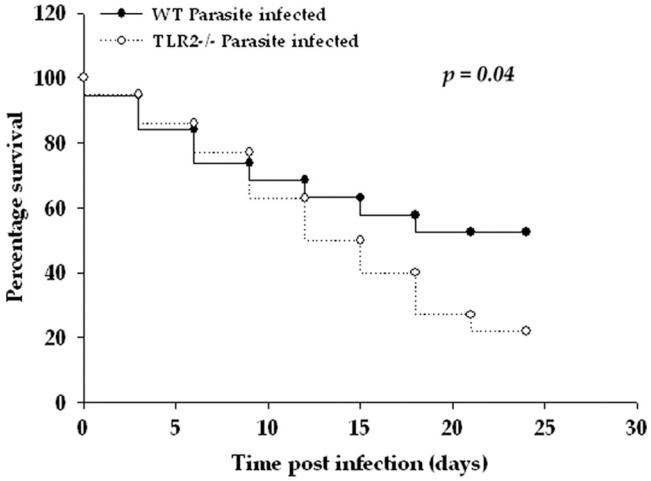

FIG. 1. TLR2$^{-/-}$ mice display increased susceptibility during murine NCC. Nineteen WT (C57BL/6) and 22 TLR2$^{-/-}$ mice were i.c. infected with 40 *M. corti* metacestodes and assessed daily for disease severity. The increased susceptibility of TLR2$^{-/-}$ mice compared to WT mice is statistically significant, as determined by Kaplan-Meier survival curve statistical analysis ($P < 0.05$).

ties, morbidity, and weight loss between 1 to 3 weeks postinfection (p.i.). In general, these overt signs appeared earlier and were more accentuated in TLR2$^{-/-}$ mice. In addition, TLR2$^{-/-}$ mice exhibited decreased survival. By 24 days after *M. corti* infection, 47% of *M. corti*-infected WT mice succumbed to the infection as opposed to 78% of TLR2$^{-/-}$ mice (17 of 22) (Fig. 1) ($P < 0.05$).

TLR2$^{-/-}$ mice exhibit increased parasite load in brain. To examine whether increased disease severity in TLR2-deficient mice was associated with less effective control of parasite growth, serial horizontal sections of infected WT and TLR2$^{-/-}$ brains of mice were stained with H&E, and the number of *M. corti* metacestodes was determined by microscopic analysis. TLR2$^{-/-}$ mice appeared less able to control parasite burdens as the brains of these mice exhibited increased numbers of parasites compared to the infected brains of WT mice (Fig. 2A). Additionally, the absence of TLR2 appeared to cause preferential sequestration of the parasites into brain parenchyma (Fig. 2B). By 3 weeks p.i., TLR2$^{-/-}$ mice exhibited a ratio of parenchymal to extraparenchymal parasites of 10:1 versus 2:1 for WT mice, suggesting that TLR2-dependent responses may influence invasiveness as well as parasite growth in the CNS.

TLR2$^{-/-}$ mice display increased CNS pathology after *M. corti* infection. H&E staining was performed to determine immunopathological changes in WT and TLR2$^{-/-}$ mice (Fig. 3). Figure 3A1 and A2 depict normal brain tissue morphology in WT and TLR2$^{-/-}$ control animals i.c. inoculated with HBSS. In contrast, strong inflammatory responses characterized by the presence of a large number of infiltrating immune cells (Fig. 3B1) and perivascular lymphocytic cuffing around blood vessels (Fig. 3C1) were observed in WT mice. In these parasite-infected WT mice, the majority of parenchymal parasites (indicated by P in Fig. 3D1 were surrounded by inflammatory leukocytes. These immunopathological events were evident at both 1 week and 3 weeks p.i. although the intensity was greater at 3 weeks p.i. In contrast, TLR2$^{-/-}$ mice displayed lower numbers of infiltrating immune cells than the WT mice at both 1 week and 3 weeks p.i. (Fig. 3B2). This correlated with little perivascular lymphocytic cuffing around blood vessels (Fig. 3C2) and few, if any, infiltrating immune cells surrounding parenchymal parasites (Fig. 3D2).

The increased number of parasites in brains of TLR2$^{-/-}$ mice may cause increased pathology due to either the mechanical disruption of brain tissue or the metabolic activity of parasites. Luxol fast blue (LFB) staining was performed to determine changes in nervous tissue integrity in both WT and TLR2$^{-/-}$ mice (Fig. 3). Figure 3E1 and E2 depict normal brain tissue morphology in WT and TLR2$^{-/-}$ control animals i.c. inoculated with HBSS. In WT infected mice, primary and secondary microglial nodule formation was observed at 3 weeks

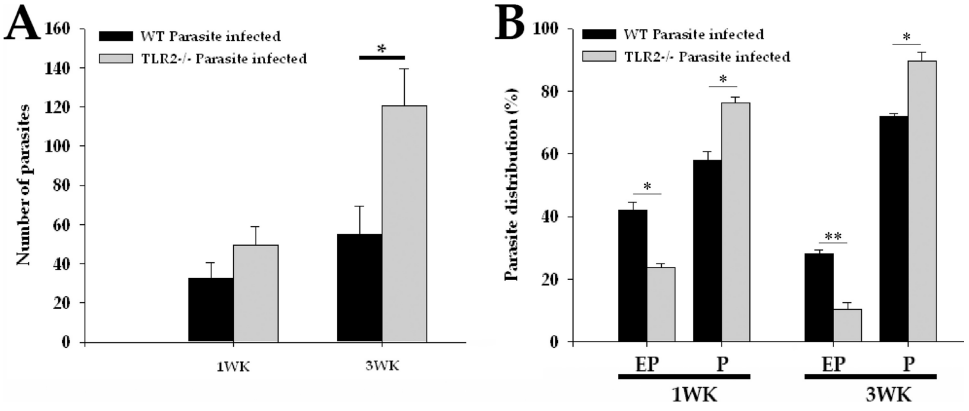

FIG. 2. TLR2$^{-/-}$ mice exhibit an increased parasite burden. WT and TLR2$^{-/-}$ were i.c. infected with ~40 *M. corti* metacestodes. At 1 week (wk) and 3 weeks p.i., WT and TLR2$^{-/-}$ mice were sacrificed. The location and number of parasites were determined by microscopic examination of serial H&E-stained brain sections. (A) Total numbers of parasites present in the brains of WT and TLR2$^{-/-}$ mice. Significant differences in parasite numbers in *M. corti*-infected TLR2$^{-/-}$ compared with the infected WT animals is denoted by an asterisk ($P < 0.05$). (B) Percentages of parasites present in parenchymal (P) and extraparenchymal (EP) regions in individual brains were calculated. Results are from three independent experiments. Significant differences in parasite numbers in *M. corti*-infected TLR2$^{-/-}$ compared with the infected WT animals are indicated (*, $P < 0.05$; **, $P < 0.005$).

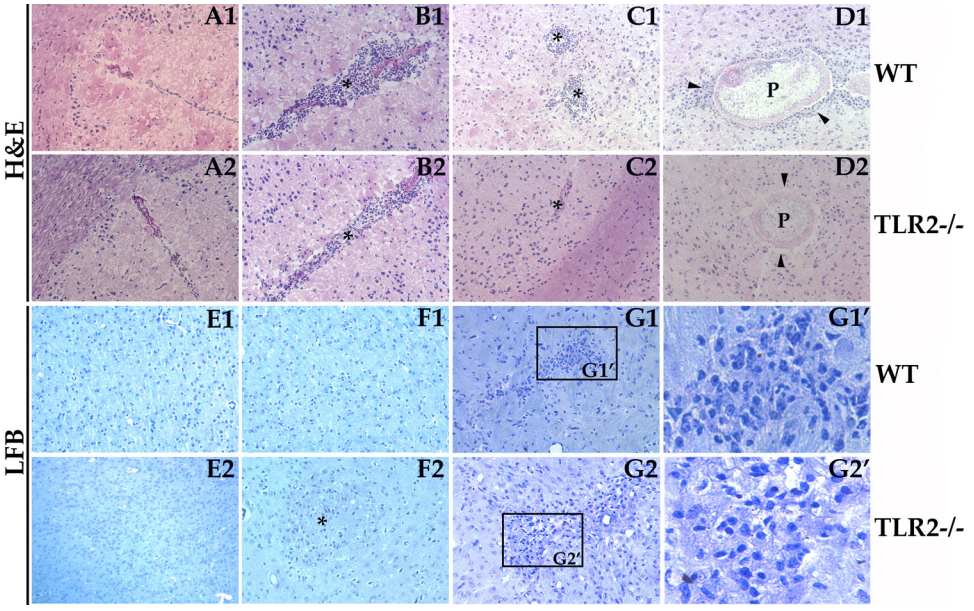

FIG. 3. Brain pathology associated with *M. corti* infection in WT and TLR2$^{-/-}$ mice. Images show H&E staining or LFB staining of brain cryosections. (A1) H&E staining showing normal parenchymal tissue in an HBSS-inoculated WT mouse. (A2) Normal parenchymal tissue in an HBSS-inoculated TLR2$^{-/-}$ mouse. (B1) Indusium griseum area of the brain in a WT mouse at 3 weeks p.i. associated with large numbers of infiltrating immune cells (*). (B2) Indusium griseum in a TLR2$^{-/-}$ mouse at 3 weeks p.i. exhibiting a reduced number of infiltrating immune cells (*). (C1) Leukocyte cuffing in a WT mouse at 3 weeks p.i. (*). (C2) Lack of leukocyte cuffing in TLR2$^{-/-}$ mice at 3 weeks p.i. (*). (D1) Parenchymal parasite (P) in a WT mouse at 3 weeks p.i. associated with infiltrating immune cells (arrowheads). (D2) Parenchymal parasite (P) in a TLR2$^{-/-}$ mouse at 3 weeks p.i. associated with absence of infiltrating immune cells (arrowheads). LFB staining shows normal parenchymal tissue in an HBSS-inoculated WT mouse (E1) and normal parenchymal tissue in an HBSS-inoculated TLR2$^{-/-}$ mouse (E2). (F1) Parenchyma of WT mouse at 1 week p.i. exhibiting absence of microglial nodule formation. (F2) Parenchyma of TLR2$^{-/-}$ mouse at 1 week p.i. exhibiting microglial nodule formation (*). (G1) Parenchyma of a WT mouse at 3 weeks p.i. exhibiting microglial nodule formation. (G1′) Boxed area in G1 depicting microglial nodule at a magnification of ×6. (G2) Parenchyma of a TLR2$^{-/-}$ mouse at 3 weeks p.i. depicting increased formation of microglial nodules that are larger than those of the WT mouse. (G2′) Boxed area in G2 depicting microglial nodule at a magnification of ×6. Results are from three independent experiments. All images are at a magnification of ×200.

p.i. (Fig. 3G1) but not at 1 week p.i. (Fig. 3F1). In contrast, in TLR2-deficient mice, microglial nodule formation was detected by 1 week p.i. (Fig. 3F2) and intensified at 3 weeks p.i. (Fig. 3G2). Parasite-infected TLR2$^{-/-}$ mice exhibited microglial nodule formations that were typically larger in number and size than those in WT infected mice at 3 weeks p.i. (Fig. 3G2), suggesting that absence of TLR2-dependent responses leads to greater CNS pathology.

TLR2$^{-/-}$ mice exhibit reduced numbers of infiltrating immune cells in the CNS. To determine whether TLR2$^{-/-}$ mice exhibit differences in numbers of infiltrating immune cells during NCC, total leukocytes from whole brains were isolated at the peak of inflammation (3 weeks p.i.) and quantified by trypan blue staining. Brains of TLR2$^{-/-}$ mice at that time exhibited significantly lower numbers of leukocytes than the WT mice ($P < 0.05$) (Fig. 4). Consistent with our previous observations (4), infiltrating leukocytes in the brains of mock-infected control mice were barely detectable.

FACS analysis was performed to examine the differences in the types of immune cells infiltrating the CNS of TLR2$^{-/-}$ and WT infected mice. Our previous studies have demonstrated that the predominant immune cells initially recruited to the brain after parasite inoculation are macrophages and γδ T cells (3 to 5 days p.i.), followed by αβ T cells (1 week p.i.) and B cells (3 weeks p.i.) (3, 11). The differences in recruitment of these immune cell types in TLR2$^{-/-}$ mice were analyzed at both an

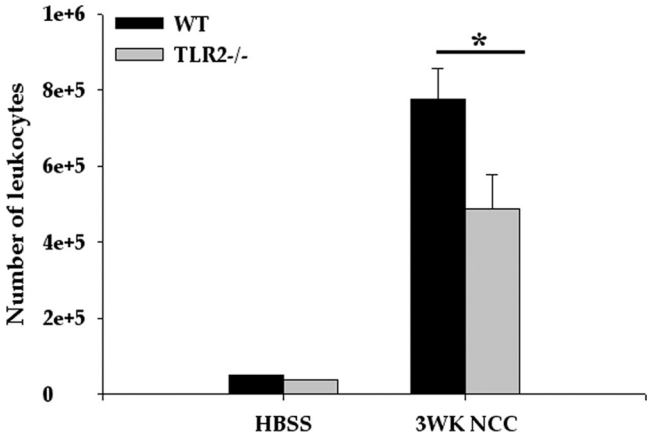

FIG. 4. TLR2$^{-/-}$ mice exhibit reduced numbers of infiltrating immune cells in CNS. WT and TLR2$^{-/-}$ mice were i.c. infected with HBSS (mock control) or *M. corti* and were sacrificed at 3 weeks p.i. Infiltrating immune cells were isolated by Ficoll Hypaque density gradient as described in Materials and Methods. Total numbers of viable immune cells in mock-infected control and parasite-infected brains of both WT and TLR2$^{-/-}$ mice were counted by trypan blue exclusion staining ($n = 4$). A significant difference in numbers of immune cells recovered from TLR2$^{-/-}$ versus WT animals is indicated by an asterisk ($P < 0.005$).

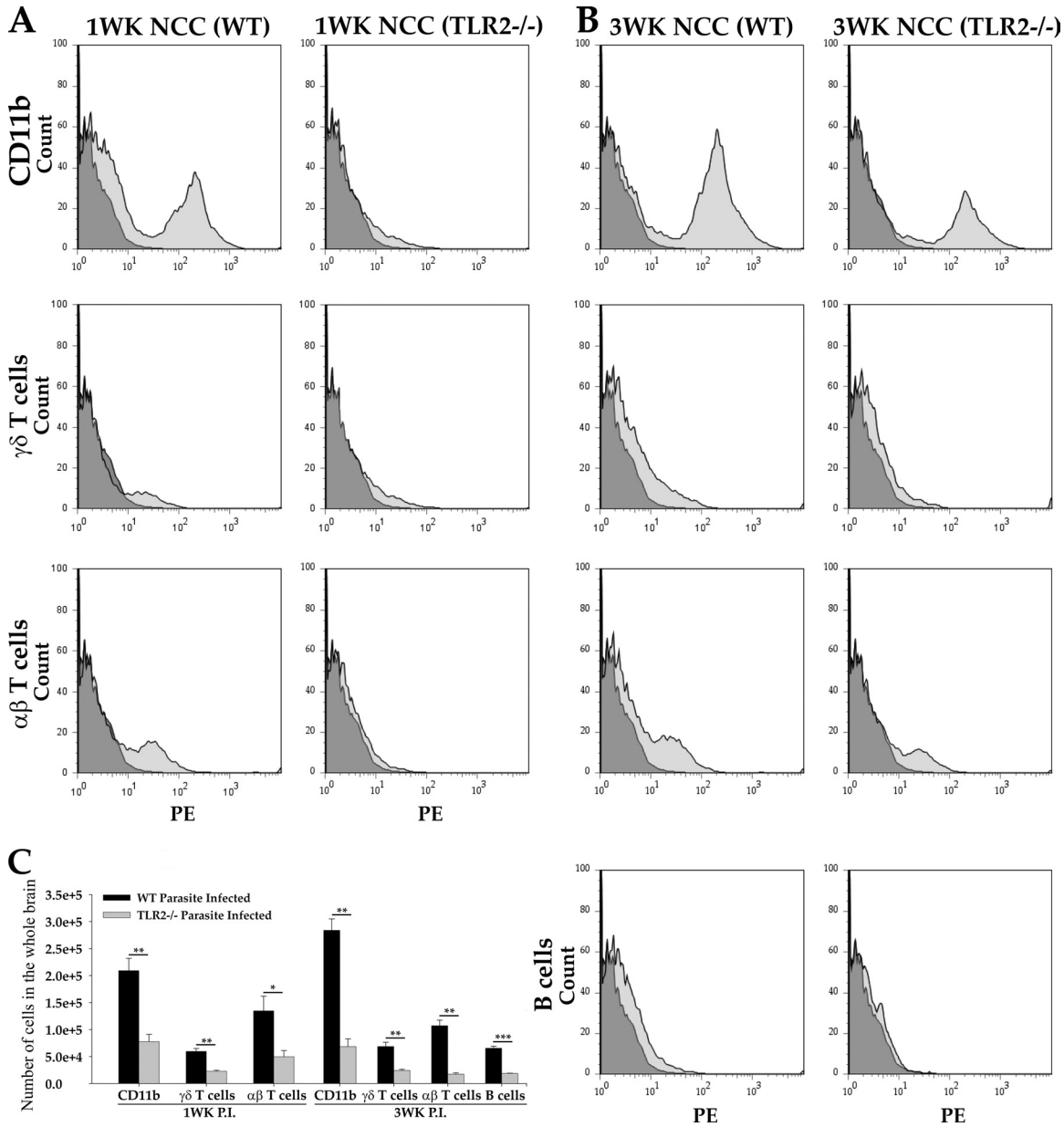

FIG. 5. TLR2$^{-/-}$ mice exhibit reduced numbers of various infiltrating immune cells in CNS. WT and TLR2$^{-/-}$ mice were i.c. infected with *M. corti* and were sacrificed at 1 week and 3 weeks p.i. Infiltrating immune cells were isolated by Ficoll Hypaque density gradient as described in Materials and Methods. Total numbers of viable immune cells in parasite-infected brains of WT and TLR2$^{-/-}$ mice were counted by trypan blue staining. (A) In each experiment, brain leukocytes from 1-week parasite-infected WT and TLR2$^{-/-}$ mice were isolated from 3 mice and pooled together. The percentages of immune cell types that were macrophages/microglia (CD11b^{+}), γδ T cells (T-cell receptor [TCR] δ2 chain-positive), αβ T cells (TCR β chain-positive), and B cells (CD19^{+}) were quantified by FACS analysis. A representative of three independent experiments is shown. (B) Brain leukocytes from 3-week parasite-infected WT and TLR2$^{-/-}$ mice were isolated from 3 mice and pooled together. FACS analysis shows a reduced number of macrophages/microglia (CD11b^{+}), γδ T cells (TCR δ2 chain-positive), and αβ T cells (TCR β chain-positive) in TLR2$^{-/-}$ mice. A representative of three independent experiments is shown. (C) Results obtained from FACS analyses are expressed as the mean ± standard error of the mean from three independent experiments. Significant differences in numbers of individual immune cells recovered from TLR2$^{-/-}$ versus WT animals are denoted by asterisks (*, $P < 0.05$; **, $P < 0.005$; ***, $P < 0.005$).

early stage of infection (1 week p.i.) and at the peak of inflammation (3 weeks p.i.) (Fig. 5). *M. corti* infection in both WT and TLR2$^{-/-}$ mice resulted in infiltration of predominantly CD11b^{+} immune cells at both 1 week and 3 weeks p.i. (Fig. 5). However, infected TLR2$^{-/-}$ mice displayed significantly lower numbers of CD11b^{+} cells at both 1 week (Fig. 5A and C) and at 3 weeks p.i. (Fig. 5B and C). Additionally, there were significantly lower numbers of γδ T cells and αβ T cells detected in TLR2$^{-/-}$ mice at 1 week (Fig. 5A and C) as well as at 3 weeks p.i. (Fig. 5B and C) than in the WT mice. In addition, CD19^{+} B cells were detected at lower levels at 3 weeks p.i. in TLR2$^{-/-}$ infected mice than in WT mice (Fig. 5B and C) but

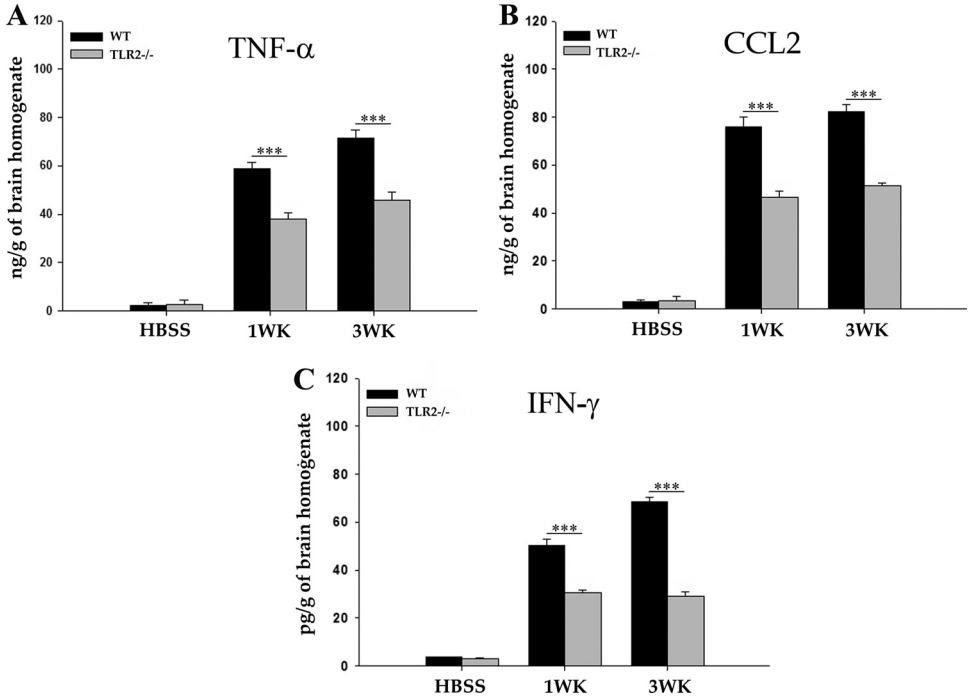

FIG. 6. TLR2$^{-/-}$ mice exhibit reduced CNS expression levels of several proinflammatory mediators. The brains from mock-infected control and *M. corti*-infected WT and TLR2$^{-/-}$ mice were harvested at 1 week and 3 weeks p.i. and homogenized in PBS with protease inhibitors (100 mg/ml), whereupon TNF-α, IFN-γ, and CCL2 protein levels were quantitated by sandwich ELISA (mean ± standard error). Results shown are the average of three infected and three mock-infected control mice for each time point. Significant differences are indicated (***, $P < 0.001$).

were undetected at 1 week p.i. in both experimental groups. This is consistent with our previously reported observations that B cells are undetected until 3 weeks p.i. in murine NCC (3). Taken together, these data demonstrate that absence of TLR2 leads to a significant reduction in leukocyte recruitment into the brain during NCC.

Immune mediators in the CNS of WT and TLR2$^{-/-}$ mice. To determine the involvement of TLR2 in proinflammatory cytokine responses after *M. corti* infection, an ELISA was performed on brain homogenates from WT and TLR2$^{-/-}$ mice. In both strains, mock-infected mouse brains displayed low basal levels of TNF-α, IFN-γ, and CCL2 (Fig. 6). Upon parasite infection, WT mice exhibited increased levels of TNF-α, IFN-γ, and CCL2 at 1 week p.i., which were further upregulated at 3 weeks p.i. (Fig. 6). In contrast, infection of TLR2$^{-/-}$ mice resulted in reduced upregulation of these cytokines. The levels of TNF-α, IFN-γ, and CCL2 in TLR2$^{-/-}$ mice were significantly lower ($P < 0.001$) than in WT infected mice at both 1 week and 3 weeks p.i. (Fig. 6). Taken together, the data suggest that induction of inflammatory mediators such as TNF-α, IFN-γ, and CCL2 is reduced in the absence of TLR2-associated signaling in murine NCC.

Our previous studies have demonstrated that early IL-6 expression in astrocytes and in their foot processes proximal to the pial vessels correlates with infiltration of leukocytes into the CNS in a region-specific manner during murine NCC (3). *M. corti*-induced TLR2 expression is also evident in astrocytes present in the same anatomical region of the brain, such as periventricular areas, and in proximity to the meninges (40). We speculate that the early induction of TLR2 in these brain regions may influence the extent of IL-6 production and contribute to leukocyte trafficking into the parasite-infected brains. Therefore, *in situ* IF microscopy was used to determine the effect of TLR2 deficiency on IL-6 expression (Fig. 7). In mock-infected brains of both WT and TLR2$^{-/-}$ mice, expression of IL-6 was detected at low basal levels in periventricular and leptomeningeal areas (Fig. 7A1 and A2). Upon parasite infection, WT mice displayed a progressive increase in the levels of IL-6 proteins, primarily in periventricular and leptomeningeal areas of the brain (Fig. 7B1). Furthermore, the upregulated expression was primarily detected on astrocytes present in these areas of the brain (Fig. 7C1), which abundantly express TLR2 (Fig. 7D1) (40), including the glia limitans in proximity to pial vessels (Fig. 7C1). In contrast, TLR2$^{-/-}$ infected mice displayed the same spatiotemporal IL-6 upregulation but at a much lower level (Fig. 7B2, and C2). Additionally, as TLR2$^{-/-}$ NCC mice display reduced leukocyte infiltration, the spatiotemporal expression of CCL3, which is a well-known leukocyte chemoattractant was analyzed by IF microscopy. In mock-infected brains of WT and TLR2$^{-/-}$ mice, CCL3 was scarcely detected (data not shown). Upon parasite infection, CCL3 (Fig. 7E1) expression was upregulated in the parenchyma of WT brain compared to a much lower level of expression in TLR2$^{-/-}$ mice (Fig. 7E2).

Parasites, particularly helminths, tend to shift the balance of immunity to a Th2 type of response that is thought to be crucial in the establishment of chronic parasitic infections. Earlier studies from our laboratory have shown that the cytokines produced in the CNS during *M. corti* infection are indicative of a mixed T helper response but with Th2 cytokines IL-4 and

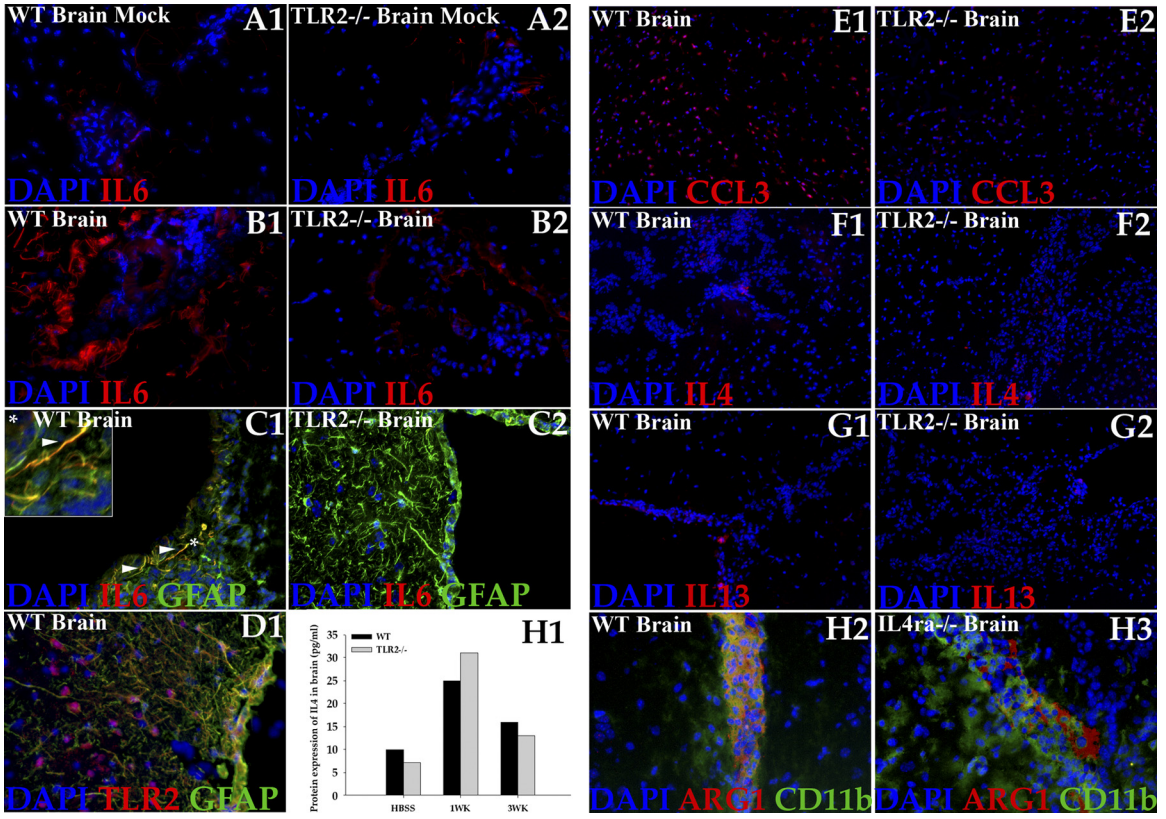

FIG. 7. Immune mediators in the CNS of WT and TLR2$^{-/-}$ mice. *In situ* IF staining was performed on frozen sections of mock-infected and parasite-infected brains of WT and TLR2$^{-/-}$ mice. IL-6, IL-4, IL-13, and ARG-1 expression was visualized in red (rhodamine RXX); astrocytes (GFAP^{+}) and myeloid cells (CD11b^{+}) were visualized in green (Alexa Fluor 488), and nuclei (blue) were stained with 4′,6′-diamidino-2-phenylindole (DAPI). IL-6 expression is shown in a representative section of a mock-infected brain from WT mouse (A1) and TLR2$^{-/-}$ mouse (A2) brain (magnification, ×400). (B1) Increased expression of IL-6 was detected in brain of a parasite-infected WT mouse at 3 weeks p.i. Magnification, ×400. (B2) Reduced IL-6 expression was detected in parasite-infected TLR2$^{-/-}$ brains at 3 weeks p.i. Magnification, ×400. (C1) IL-6 is predominantly expressed in brain astrocytes of a parasite-infected WT mouse at 3 weeks p.i. Arrowheads indicate colocalization of IL-6 and GFAP (yellow/orange). Magnification, ×400. The inset shows the selected area (∗) depicting IL-6 expression in astrocytes and their processes at a magnification of ×4. (C2) IL-6 expression is reduced in brain astrocytes of a TLR2$^{-/-}$ mouse at 3 weeks p.i. Magnification ×400. (D1) TLR2 is predominantly expressed in brain astrocytes of a parasite-infected WT mouse at 3 weeks p.i., with colocalization of TLR2 and GFAP (yellow/orange). Magnification, ×400. (E1) Increased expression of CCL3 was detected in brain parenchyma of a parasite-infected WT mouse at 3 weeks p.i. Magnification, ×200. (E2) Reduced CCL3 expression was detected in parasite-infected TLR2$^{-/-}$ brains at 3 weeks p.i. Magnification, ×200. Mild increase in expression of IL-4 was detected in parasite infected brains of WT (F1) and TLR2$^{-/-}$ (F2) mice at 3 weeks p.i. (magnification, ×200). Mild increase in expression of IL-13 was detected in parasite-infected brains of WT (G1) and TLR2$^{-/-}$ (G2) mice at 3 weeks p.i. (magnification, ×200). (H1) The brains from mock-infected control and *M. corti*-infected WT and TLR2$^{-/-}$ mice were harvested at 1 week and 3 weeks p.i. and homogenized in PBS with protease inhibitors (100 mg/ml). Protein levels of IL-4 were quantified using Luminex technology and a commercial RodentMAP assay (Rules-Based Medicine). (H2) ARG-1 expression in parasite-infected brain of a WT mouse at 2 weeks p.i. Magnification, ×400. (H3) ARG-1 expression in parasite-infected brain from IL-4Rα$^{-/-}$ mouse at 2 weeks p.i. ($n = 2$). Magnification, ×400.

IL-13 detected in relatively small amounts (11). IF microscopy was used to determine the effect of TLR2 deficiency on IL-4 and IL-13 expression in WT and TLR2$^{-/-}$ mice (Fig. 7F and G). In mock-infected brains of WT and TLR2$^{-/-}$ mice, expression of both IL-4 and IL-13 was scarcely detected (data not shown). Upon parasite infection, both WT and TLR2-deficient mice displayed a mild increase in the levels of IL-4 (Fig. 7F1 and F2) and IL-13 (Fig. 7G1 and G2). The increase was apparent in terms of both the intensity and the numbers of cells expressing them. Furthermore, quantitative determination of the IL-4 level (sensitivity of assay, 15 pg/ml), analyzed commercially by RodentMAP assay (Rules-Based Medicine), confirmed a modest upregulation of IL-4 in the CNS of both WT and TLR2-deficient mice at 1 week and 3 weeks p.i. during NCC (Fig. 7H1).

TLR2$^{-/-}$ mice display reduced expression of alternative activation macrophage markers. In CNS infections sustained inflammation is a major cause of tissue damage and associated pathology (13). Within this context, *M. corti* parasite-infected TLR2$^{-/-}$ mice display reduced inflammatory cytokines in the CNS but intriguingly exhibit greater neuropathology. Thus, it is possible that TLR2-associated responses may contribute to protective effects by regulating tissue-reparative mechanisms in NCC brains. Since tissue restoration and repair are among the well-defined regulatory properties of AAMs, the expression of AAM markers ARG-1, Fizz1, and YM1 was analyzed

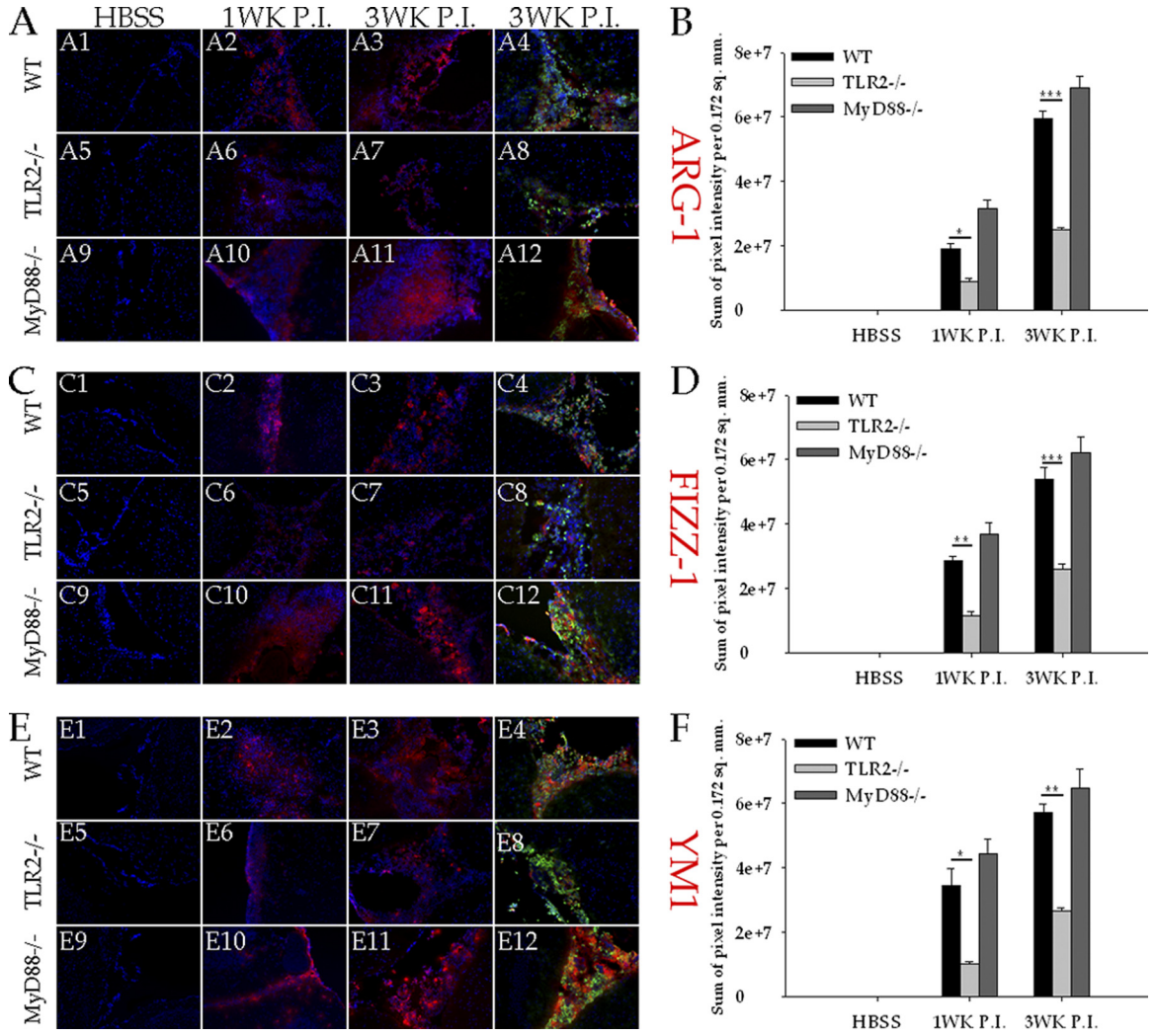

FIG. 8. TLR2$^{-/-}$ mice present reduced CNS expression levels of ARG-1, Fizz1, and YM1. *In situ* IF staining was performed on frozen sections of mock-infected and parasite-infected brains of WT and TLR2$^{-/-}$ mice at 1 week and 3 weeks p.i. ARG-1, Fizz1, and YM1 expression was visualized in red (rhodamine RXX), macrophages/microglia (CD11b^{+}) were visualized in green (Alexa Fluor 488), and nuclei were stained with DAPI (blue) (magnification, ×200). (A) ARG-1 expression in mock-infected (A1, A5, and A9), 1-week p.i. (A2, A6, and A10), and 3-week p.i. (A3, A7, and A11) brains of WT, TLR2$^{-/-}$, and MyD88$^{-/-}$ mice ARG-1 expression at 3 weeks p.i. is colocalized with CD11b^{+} staining (yellow/orange) in WT (A4), TLR2$^{-/-}$ (A8), and MyD88$^{-/-}$ (A12) NCC mouse brains. (B) The relative levels of ARG-1 expression in mock- and *M. corti*-infected WT, TLR2$^{-/-}$, or MyD88$^{-/-}$ animals were calculated as described in Materials and Methods. Significant differences are denoted by asterisks (*, $P < 0.05$; **, $P < 0.005$; ***, $P < 0.005$). (C) Fizz1 expression in mock-infected (C1, C5, and C9), 1-week p.i. (C2, C6, and C10), and 3-week p.i. (C3, C7, and C11) brains of WT, TLR2$^{-/-}$, and MyD88$^{-/-}$ mice. Fizz1 expression at 3 weeks p.i. is colocalized with CD11b^{+} staining (yellow/orange) in WT (C4), TLR2$^{-/-}$ (C8), and MyD88$^{-/-}$ (C12) NCC mouse brains. (D) The relative levels of Fizz1 expression in mock- and *M. corti*-infected WT, TLR2$^{-/-}$, or MyD88$^{-/-}$ animals were calculated as described in Materials and Methods. Significant differences are denoted by asterisks (*, $P < 0.05$; **, $P < 0.005$; ***, $P < 0.005$). (E) YM1 expression in mock-infected (E1, E5, and E9), 1-week p.i. (E2, E6, and E10), and 3-week p.i. (E3, E7, and E11) brains of WT, TLR2$^{-/-}$, and MyD88$^{-/-}$ mice. YM1 expression at 3 weeks p.i. is colocalized with CD11b^{+} staining (yellow/orange) in WT (E4), TLR2$^{-/-}$ (E8), and MyD88$^{-/-}$ (E12) NCC mouse brains. (F) The relative levels of YM1 expression in mock- and *M. corti*-infected WT, TLR2$^{-/-}$, or MyD88$^{-/-}$ animals were calculated as described in Materials and Methods. Significant differences are denoted by asterisks (*, $P < 0.05$; **, $P < 0.005$; ***, $P < 0.005$).

by *in situ* IF microscopy. In mock-infected brains of both WT and TLR2$^{-/-}$ mice, ARG-1 (Fig. 8A1 and A5), Fizz1 (Fig. 8C1 and C5), and YM1 (Fig. 8E1 and E5) were scarcely detected. Upon infection, ARG-1 (Fig. 8A2), Fizz1 (Fig. 8C2), and YM1 (Fig. 8E2) expression levels were upregulated in the WT brain after *M. corti* infection at 1 week p.i. The expression remained high, as indicated by extensive staining for ARG-1 (Fig. 8A3) Fizz1 (Fig. 8C3), and ARG-1 (Fig. 8E3) at 3 weeks p.i. Additionally, ARG-1 (Fig. 8A4), Fizz-1 (Fig. 8C4), and YM1 (Fig. 8E4) were mostly detected in brain areas associated with infiltrating leukocytes at all the time points analyzed (Fig. 8). Interestingly, the upregulated expression of these molecules was also associated with their increased secretion, as determined by their presence in cell-free regions (data not shown). In contrast, infected TLR2-deficient mice exhibited substantially less expression of ARG-1 at both 1 week (Fig. 8A6) and 3 weeks p.i. (Fig. 8A7) than WT mice (Fig. 8A2 and A3). Infected TLR2-deficient mice displayed significantly lower lev-

els of Fizz1 at 1 week (Fig. 8C6) and 3 weeks p.i. (Fig. 8C7) than infected WT mice (Fig. 8C2 and C3). Similarly, infected TLR2-deficient mice also displayed significantly lower levels of YM1 at 1 week (Fig. 8E6) and 3 weeks p.i. (Fig. 8E7) than infected WT mice (Fig. 8E2 and E3). Such decreases were quantified by measurement of mean pixel intensity of ARG-1 (Fig. 8B), Fizz1 (Fig. 8D), and YM1 staining (Fig. 8F). Double immunofluorescence staining of Fizz1 or ARG-1 with CD11b indicated that the majority of cells positive for ARG-1 (Fig. 8A4), Fizz1 (Fig. 8C4), and YM1 (Fig. 8E4) in WT infected mice were $CD11b^+$ myeloid cells. In contrast, $TLR2^{-/-}$ mice displayed minimal expression of these AAM markers, including in areas containing considerable numbers of $CD11b^+$ cells (Fig. 8A8, C8, and E8).

Our previous studies have demonstrated that mice deficient in MyD88, an adaptor molecule necessary for signal transduction through most of the TLRs including TLR2 (47), exhibit reduced pathological signs and are less susceptible to the infection during NCC (39). To determine the extent to which AAM-associated responses correlate with reduced disease severity after *M. corti* infection in these mice, double IF staining of CD11b with AAM markers, YM1, Fizz1, and ARG-1, was performed. Similar to results in the WT (Fig. 8A, C, and E), mock-infected brains of $MyD88^{-/-}$ mice displayed scarce expression of ARG-1 (Fig. 8A9), Fizz1 (Fig. C9), and YM1 (Fig. 8E9). After parasite infection, $MyD88^{-/-}$ mice displayed expression of ARG-1 (Fig. 8A10 and A11), Fizz1 (Fig. 8C10 and C11), and YM1 (Fig. 8E10 and E11) at similar or higher levels than those in WT NCC mice (Fig. 8A2, A3, C3, C4, E3, and E4). Quantification of the mean pixel intensity of ARG-1 (Fig. 8B), Fizz1 (Fig. 8D), and YM1 (Fig. 8F) staining confirmed these observations.

Th2 cytokines IL-4 and IL-13 are known to induce markers associated with AAMs in helminth infections (23, 27). However, these cytokines are detected in relatively small amounts in the CNS during murine NCC (Fig. 7F, G, and H1) (11). To determine the role of these Th2 cytokines in the development of cells with AAM phenotypes in the CNS during NCC, the expression of ARG-1 and YM1 was analyzed in $IL\text{-}4R\alpha^{-/-}$ mice (receptor for both IL-4 and IL-13). The expression of ARG-1 (Fig. 7H2 and H3) and YM1 (data not shown) was partially downregulated in $IL\text{-}4R\alpha^{-/-}$ mice but could be detected in many $CD11b^+$ myeloid cells.

DISCUSSION

An important step in eliciting pathogen-specific immune responses in the brain is the induction of inflammatory responses with leukocyte infiltration into the CNS (50). Recent studies have demonstrated the role of TLRs in orchestrating an inflammatory cascade in various models of CNS infectious diseases (28, 31), including bacterial meningitis (30), brain abscess (19, 44), and viral (59) and parasitic infections (38). We have shown that TLR2 is upregulated within 1 to 2 days in the CNS of mice infected i.c. with *M. corti* (40). We hypothesized that this early upregulation of TLR2 is involved in initial innate immune responses providing necessary signals for subsequent adaptive immune responses. Indeed, results presented here show a reduction in the infiltration of immune cells (macrophages, γδ T cells, and αβ T cells) as well as decreased proinflammatory cytokine responses after *M. corti* infection in $TLR2^{-/-}$ mice compared with levels in WT mice. Interestingly, much of the upregulation of TLR2 during infection is associated with astrocytes in the glia limitans (40), the outermost layer of the proper nervous tissue (50). These areas contain pial vessels that have weaker barrier properties and are often the first to be invaded by pathogens (50). This is the likely source of TLR2 ligands for the tangential astrocytes of the glia limitans. This is in keeping with the reduced IL-6 expression observed in astrocytes of $TLR2^{-/-}$ in these areas compared with levels in the WT. Moreover, our previous studies showed that IL-6 expression by astrocytes in the glial limitans in proximity to pial vessels correlates with leukocyte migration through pial vessels in adjoining extraparenchymal spaces during murine NCC (3). Taken together, the results strongly support a role for TLR2-associated signaling in the development of the initial inflammatory response in the CNS as a result of *M. corti* infection.

A growing body of evidence indicates that TLRs participate in the recognition of parasitic infections and elicit early immune responses (9, 14, 56). In experimental models involving parasitic infections, mice deficient in TLRs display reduced levels of the Th1 inflammatory mediators IL-12p40 and/or IFN-γ, which correlate with reduced parasite clearance and increased disease severity (22, 38). Of particular interest are studies of experimental cysticercosis in which mice are infected intraperitoneally with the larval stage of *Taenia crassiceps* and parasite containment requires Th1-type responses and nitric oxide production (1, 54). Likewise, the results from the present study suggest that decreased expression of proinflammatory cytokines, including TNF-α and IFN-γ, correlates with reduced parasite clearance, particularly in brain parenchyma. As TLR2 is abundantly expressed in nervous tissue cells, it is possible that the reduced degree of production of inflammatory cytokines in the parenchymal versus extraparenchymal region results in increased parasite sequestration to brain parenchyma of $TLR2^{-/-}$ mice. However, the relative contribution of inflammatory cytokines to parasite containment in the CNS is uncertain. Our recent observations show that infection of mice lacking STAT6 (signal transducer and activator of transcription 6), a prominent regulator of AAM development (34), results in the significant upregulation of the Th1 effector molecule inducible nitrous oxide synthase (iNOS) in the CNS yet results in increased parasite burdens in brain parenchyma (37). In addition, $STAT6^{-/-}$ NCC mice exhibit decreased numbers of AAMs in the CNS and increased disease severity compared to WT mice. As both $TLR2^{-/-}$ and $STAT6^{-/-}$ infected mice exhibit a reduction of AAMs and lower survival rates, AAMs may play a protective role. This is consistent with a recent study showing that $IL\text{-}4^{-/-}$ mice infected i.p. with *M. corti* display a reduction in the number of ARG-1-expressing AAMs as well as higher parasite burdens, tissue pathology, and a significantly increased susceptibility to infection (45). Moreover, studies involving other parasite infections have also reported that AAM-associated responses mediate parasite clearance and host protection (6, 20, 21, 54). Taking these results together, it is possible that TLR2-dependent AAM-associated responses play a contributing role in limiting disease severity in murine NCC.

In contrast to $TLR2^{-/-}$ mice, $MyD88^{-/-}$ mice displayed

increased expression of all the three AAM-associated markers compared to levels in the WT mice. Besides TLR2, MyD88 also interacts with other TLRs and several other TIR domain-containing receptors (8) and non-TIR domain-containing receptors (25, 43, 46, 60, 61). Interestingly, in contrast to TLR2$^{-/-}$ mice, *M. corti*-infected MyD88$^{-/-}$ mice had reduced pathological signs and decreased susceptibility to the infection (39). Similar to our findings, a recent study demonstrated that *Leishmania braziliensis*-infected TLR2$^{-/-}$ and MyD88$^{-/-}$ mice exhibit differential disease outcomes (62). Thus, MyD88$^{-/-}$ infected mice were more susceptible to infection, and dendritic cells from infected MyD88$^{-/-}$ mice produced less proinflammatory cytokines than those of WT mice. In contrast, TLR2$^{-/-}$ mice were able to control the infection and produced more inflammatory cytokines than their WT counterparts (62). This is intriguing as MyD88 is a primary adaptor molecule involved in downstream signaling originating from TLR2. However, contrasting outcomes in TLR2$^{-/-}$ and MyD88$^{-/-}$ infected mice in NCC and *L. braziliensis* infection suggest a possibility of TLR2 functioning as a coreceptor with another pattern recognition receptor (PRR) or perhaps the involvement of an unknown MyD88-independent pathway. Nonetheless, it is likely that TLR2 is selectively involved in immune regulatory mechanisms in NCC.

Helminth parasites tend to shift the balance of immunity to a Th2-type (IL-4 or IL-13) or IL-10-type response that activates or expands AAMs (23, 27). Thus, the AAMs M2a (induced by IL-4/IL-13) (42, 48) and M2c (induced by IL-10) (33), but not M2b (induced by combined exposure to immune complexes and TLR or IL-1R agonists) (41), are thought to play an important role specifically in helminth infections. However, the cytokines produced in the CNS during *M. corti* infection are indicative of a mixed T helper response but with IL-4, IL-13, and IL-10 detected in relatively small amounts (11). Moreover, the expression of AAM-associated markers in IL-4R$\alpha^{-/-}$ mice is partially affected while in IL-10$^{-/-}$ mice it seems to be largely unaffected (unpublished results). This suggests that IL-4 and IL-13, but not IL-10, may play a contributing role in development of the AAM phenotype. However, a reduction in cells with AAM phenotypes after *M. corti* infection in TLR2-deficient mice compared to levels in WT mice suggests possible involvement of innate immune pathways in the development of AAMs. In support of this, recent evidence indicates that TLR2-associated responses can lead to AAM development upon bacterial infection of macrophages (18, 58). In the absence of a dominant Th2 or IL-10 response in the CNS during murine NCC, it is possible that TLR2-associated production of other regulatory cytokines drives AAM development. Alternatively, parasite antigens secreted by *M. corti* may directly interact with host innate receptors and contribute to the development of the AAM phenotype. In this regard, schistosomal lacto-*N*-fucopentaose III (LNFPIII) glycan antigens have been identified to upregulate expression of AAM-associated markers in IL-4R$\alpha^{-/-}$ mice, suggesting existence of an innate pathway for development of AAMs (7). Our studies have demonstrated that *T. solium* and *M. corti* larvae have teguments rich in glycan antigens that, during CNS infection, are shed and taken up by host cells in the CNS environment (2). We speculate that recognition of parasite glycans by TLR2 and coreceptors, particularly C-type lectin receptors (CLR), the major PRRs involved in glycan antigen recognition, might be involved in this process. Currently, we are testing putative parasite-derived glycan antigens which may have a role in the development of AAMs and innate immune mechanisms involved in this process.

The present study demonstrates that TLR2 functions in promoting AAM-associated responses in the CNS microenvironment that are involved in limiting parasite growth in brain parenchyma and possibly heal nervous tissue injury. Our previous studies have identified that in γδ T$^{-/-}$ or MyD88$^{-/-}$ NCC mice, a reduced inflammatory response is associated with decreased mortality and morbidity, suggesting that a hyperinflammatory response contributes to neuropathology and disease severity in NCC (38, 39). Taking into consideration the results from this study, we additionally propose that AAM-associated responses in the CNS are also involved in modulating neuropathology and disease severity in NCC. Collectively, the present study demonstrates that TLR2 functions in regulating immunity in the CNS microenvironment, resulting in diminished disease severity in murine NCC.

ACKNOWLEDGMENTS

This work was supported by awards NS 35974, AI 59703, and P01 AI 057986 from the National Institutes of Health.

We declare that we have no financial conflicts of interest.

REFERENCES

1. **Alonso-Trujillo, J., I. Rivera-Montoya, M. Rodriguez-Sosa, and L. I. Terrazas.** 2007. Nitric oxide contributes to host resistance against experimental *Taenia crassiceps* cysticercosis. Parasitol. Res. **100:**1341–1350.
2. **Alvarez, J. I., J. Rivera, and J. M. Teale.** 2008. Differential release and phagocytosis of tegument glycoconjugates in neurocysticercosis: implications for immune evasion strategies. PLoS Negl. Trop. Dis. **2:**e218.
3. **Alvarez, J. I., and J. M. Teale.** 2006. Breakdown of the blood brain barrier and blood-cerebrospinal fluid barrier is associated with differential leukocyte migration in distinct compartments of the CNS during the course of murine NCC. J. Neuroimmunol. **173:**45–55.
4. **Alvarez, J. I., and J. M. Teale.** 2007. Differential changes in junctional complex proteins suggest the ependymal lining as the main source of leukocyte infiltration into ventricles in murine neurocysticercosis. J. Neuroimmunol. **187:**102–113.
5. **Alvarez, J. I., and J. M. Teale.** 2007. Evidence for differential changes of junctional complex proteins in murine neurocysticercosis dependent upon CNS vasculature. Brain Res. **1169:**98–111.
6. **Anthony, R. M., et al.** 2006. Memory T(H)2 cells induce alternatively activated macrophages to mediate protection against nematode parasites. Nat. Med. **12:**955–960.
7. **Atochina, O., A. A. Da'dara, M. Walker, and D. A. Harn.** 2008. The immunomodulatory glycan LNFPIII initiates alternative activation of murine macrophages in vivo. Immunology **125:**111–121.
8. **Boraschi, D., and A. Tagliabue.** 2006. The interleukin-1 receptor family. Vitam. Horm. **74:**229–254.
9. **Campos, M. A., et al.** 2004. Impaired production of proinflammatory cytokines and host resistance to acute infection with *Trypanosoma cruzi* in mice lacking functional myeloid differentiation factor 88. J. Immunol. **172:**1711–1718.
10. **Cardona, A. E., P. A. Gonzalez, and J. M. Teale.** 2003. CC chemokines mediate leukocyte trafficking into the central nervous system during murine neurocysticercosis: role of γδ T cells in amplification of the host immune response. Infect. Immun. **71:**2634–2642.
11. **Cardona, A. E., B. I. Restrepo, J. M. Jaramillo, and J. M. Teale.** 1999. Development of an animal model for neurocysticercosis: immune response in the central nervous system is characterized by a predominance of γδ T cells. J. Immunol. **162:**995–1002.
12. **Cardona, A. E., and J. M. Teale.** 2002. γ/δ T cell-deficient mice exhibit reduced disease severity and decreased inflammatory response in the brain in murine neurocysticercosis. J. Immunol. **169:**3163–3171.
13. **Chavarria, A., and J. Alcocer-Varela.** 2004. Is damage in central nervous system due to inflammation? Autoimmun. Rev. **3:**251–260.
14. **Del Rio, L., et al.** 2004. *Toxoplasma gondii* triggers myeloid differentiation factor 88-dependent IL-12 and chemokine ligand 2 (monocyte chemoattractant protein 1) responses using distinct parasite molecules and host receptors. J. Immunol. **172:**6954–6960.

15. **Didierlaurent, A., et al.** 2004. Flagellin promotes myeloid differentiation factor 88-dependent development of Th2-type response. J. Immunol. **172:** 6922–6930.
16. **Dillon, S., et al.** 2004. A Toll-like receptor 2 ligand stimulates Th2 responses in vivo, via induction of extracellular signal-regulated kinase mitogen-activated protein kinase and c-Fos in dendritic cells. J. Immunol. **172:**4733–4743.
17. **Drennan, M. B., et al.** 2005. The induction of a type 1 immune response following a *Trypanosoma brucei* infection is MyD88 dependent. J. Immunol. **175:**2501–2509.
18. **El Kasmi, K. C., et al.** 2008. Toll-like receptor-induced arginase 1 in macrophages thwarts effective immunity against intracellular pathogens. Nat. Immunol. **9:**1399–1406.
19. **Esen, N., and T. Kielian.** 2009. Toll-like receptors in brain abscess. Curr. Top. Microbiol. Immunol. **336:**41–61.
20. **Finkelman, F. D., et al.** 2004. Interleukin-4- and interleukin-13-mediated host protection against intestinal nematode parasites. Immunol. Rev. **201:** 139–155.
21. **Gause, W. C., J. F. Urban, Jr., and M. J. Stadecker.** 2003. The immune response to parasitic helminths: insights from murine models. Trends Immunol. **24:**269–277.
22. **Gazzinelli, R. T., and E. Y. Denkers.** 2006. Protozoan encounters with Toll-like receptor signalling pathways: implications for host parasitism. Nat. Rev. Immunol. **6:**895–906.
23. **Harn, D. A., J. McDonald, O. Atochina, and A. A. Da'dara.** 2009. Modulation of host immune responses by helminth glycans. Immunol. Rev. **230:**247–257.
24. **Hoebe, K., E. Janssen, and B. Beutler.** 2004. The interface between innate and adaptive immunity. Nat. Immunol. **5:**971–974.
25. **Honda, K., et al.** 2004. Role of a transductional-transcriptional processor complex involving MyD88 and IRF-7 in Toll-like receptor signaling. Proc. Natl. Acad. Sci. U. S. A. **101:**15416–15421.
26. **Irani, D. N., and D. E. Griffin.** 1991. Isolation of brain parenchymal lymphocytes for flow cytometric analysis. Application to acute viral encephalitis. J. Immunol. Methods **139:**223–231.
27. **Jenkins, S. J., and J. E. Allen.** 2010. Similarity and diversity in macrophage activation by nematodes, trematodes, and cestodes. J. Biomed. Biotechnol. **2010:**262609.
28. **Kielian, T.** 2009. Overview of toll-like receptors in the CNS. Curr. Top. Microbiol. Immunol. **336:**1–14.
29. **Kluver, H., and E. Barrera.** 1953. A method for the combined staining of cells and fibers in the nervous system. J. Neuropathol. Exp. Neurol. **12:**400–403.
30. **Koedel, U.** 2009. Toll-like receptors in bacterial meningitis. Curr. Top. Microbiol. Immunol. **336:**15–40.
31. **Lehnardt, S.** 2010. Innate immunity and neuroinflammation in the CNS: the role of microglia in Toll-like receptor-mediated neuronal injury. Glia **58:** 253–263.
32. **Mahanty, S., and H. H. Garcia.** 2010. Cysticercosis and neurocysticercosis as pathogens affecting the nervous system. Prog. Neurobiol. **91:**172–184.
33. **Mantovani, A., et al.** 2004. The chemokine system in diverse forms of macrophage activation and polarization. Trends Immunol. **25:**677–686.
34. **Martinez, F. O., L. Helming, and S. Gordon.** 2009. Alternative activation of macrophages: an immunologic functional perspective. Annu. Rev. Immunol. **27:**451–483.
35. **McDermott, E. P., and L. A. O'Neill.** 2002. Ras participates in the activation of p38 MAPK by interleukin-1 by associating with IRAK, IRAK2, TRAF6, and TAK-1. J. Biol. Chem. **277:**7808–7815.
36. **Mishra, B. B., U. M. Gundra, and J. M. Teale.** 2008. Expression and distribution of Toll-like receptors 11–13 in the brain during murine neurocysticercosis. J. Neuroinflammation **5:**53.
37. **Mishra, B. B., U. M. Gundra, and J. M. Teale.** 2011. STAT6$^{-/-}$ mice exhibit decreased cells with alternatively activated macrophage phenotypes and enhanced disease severity in murine neurocysticercosis. J. Neuroimmunol. **232:** 26–34.
38. **Mishra, B. B., U. M. Gundra, and J. M. Teale.** 2009. Toll-like receptors in CNS parasitic infections. Curr. Top. Microbiol. Immunol. **336:**83–104.
39. **Mishra, B. B., U. M. Gundra, K. Wong, and J. M. Teale.** 2009. MyD88-deficient mice exhibit decreased parasite induced immune responses but reduced disease severity in a murine model of neurocysticercosis. Infect. Immun. **77:**5369–5379.
40. **Mishra, B. B., P. K. Mishra, and J. M. Teale.** 2006. Expression and distribution of Toll-like receptors in the brain during murine neurocysticercosis. J. Neuroimmunol. **181:**46–56.
41. **Mosser, D. M.** 2003. The many faces of macrophage activation. J. Leukoc. Biol. **73:**209–212.
42. **Munder, M., K. Eichmann, and M. Modolell.** 1998. Alternative metabolic states in murine macrophages reflected by the nitric oxide synthase/arginase balance: competitive regulation by CD4$^+$ T cells correlates with Th1/Th2 phenotype. J. Immunol. **160:**5347–5354.
43. **Negishi, H., et al.** 2006. Evidence for licensing of IFN-gamma-induced IFN regulatory factor 1 transcription factor by MyD88 in Toll-like receptor-dependent gene induction program. Proc. Natl. Acad. Sci. U. S. A. **103:** 15136–15141.
44. **Nichols, J. R., et al.** 2009. TLR2 deficiency leads to increased Th17 infiltrates in experimental brain abscesses. J. Immunol. **182:**7119–7130.
45. **O'Connell, A. E., et al.** 2009. IL-4$^{-/-}$ mice with lethal *Mesocestoides corti* infections–reduced Th2 cytokines and alternatively activated macrophages. Parasite Immunol. **31:**741–749.
46. **Ojaniemi, M., et al.** 2003. Phosphatidylinositol 3-kinase is involved in Toll-like receptor 4-mediated cytokine expression in mouse macrophages. Eur. J. Immunol. **33:**597–605.
47. **O'Neill, L. A., and A. G. Bowie.** 2007. The family of five: TIR-domain-containing adaptors in Toll-like receptor signalling. Nat. Rev. Immunol. **7:**353–364.
48. **Pauleau, A. L., et al.** 2004. Enhancer-mediated control of macrophage-specific arginase I expression. J. Immunol. **172:**7565–7573.
49. **Piggott, D. A., et al.** 2005. MyD88-dependent induction of allergic Th2 responses to intranasal antigen. J. Clin. Invest. **115:**459–467.
50. **Ransohoff, R. M., P. Kivisakk, and G. Kidd.** 2003. Three or more routes for leukocyte migration into the central nervous system. Nat. Rev. Immunol. **3:**569–581.
51. **Redecke, V., et al.** 2004. Cutting edge: activation of Toll-like receptor 2 induces a Th2 immune response and promotes experimental asthma. J. Immunol. **172:**2739–2743.
52. **Restrepo, B. I., et al.** 2001. Brain granulomas in neurocysticercosis patients are associated with a Th1 and Th2 profile. Infect. Immun. **69:**4554–4560.
53. **Restrepo, B. I., P. Llaguno, M. A. Sandoval, J. A. Enciso, and J. M. Teale.** 1998. Analysis of immune lesions in neurocysticercosis patients: central nervous system response to helminth appears Th1-like instead of Th2. J. Neuroimmunol. **89:**64–72.
54. **Reyes, J. L., and L. I. Terrazas.** 2007. The divergent roles of alternatively activated macrophages in helminthic infections. Parasite Immunol. **29:**609–619.
55. **Rock, F. L., G. Hardiman, J. C. Timans, R. A. Kastelein, and J. F. Bazan.** 1998. A family of human receptors structurally related to *Drosophila* Toll. Proc. Natl. Acad. Sci. U. S. A. **95:**588–593.
56. **Scanga, C. A., et al.** 2002. Cutting edge: MyD88 is required for resistance to *Toxoplasma gondii* infection and regulates parasite-induced IL-12 production by dendritic cells. J. Immunol. **168:**5997–6001.
57. **Sciutto, E., A. Chavarria, G. Fragoso, A. Fleury, and C. Larralde.** 2007. The immune response in *Taenia solium* cysticercosis: protection and injury. Parasite Immunol. **29:**621–636.
58. **Shirey, K. A., L. E. Cole, A. D. Keegan, and S. N. Vogel.** 2008. *Francisella tularensis* live vaccine strain induces macrophage alternative activation as a survival mechanism. J. Immunol. **181:**4159–4167.
59. **Suh, H. S., C. F. Brosnan, and S. C. Lee.** 2009. Toll-like receptors in CNS viral infections. Curr. Top. Microbiol. Immunol. **336:**63–81.
60. **Sun, D., and A. Ding.** 2006. MyD88-mediated stabilization of interferon-gamma-induced cytokine and chemokine mRNA. Nat. Immunol. **7:**375–381.
61. **Takaoka, A., et al.** 2005. Integral role of IRF-5 in the gene induction programme activated by Toll-like receptors. Nature **434:**243–249.
62. **Vargas-Inchaustegui, D. A., et al.** 2009. Distinct roles for MyD88 and Toll-like receptor 2 during *Leishmania braziliensis* infection in mice. Infect. Immun. **77:**2948–2956.
63. **White, A. C.** 2000. Neurocysticercosis: updates on epidemiology, pathogenesis, diagnosis, and management. Annu. Rev. Med. **51:**187–206.
64. **White, A. C., Jr.** 1997. Neurocysticercosis: a major cause of neurological disease worldwide. Clin. Infect. Dis. **24:**101–115.
65. **White, A. C., Jr., P. Robinson, and R. Kuhn.** 1997. Taenia solium cysticercosis: host-parasite interactions and the immune response. Chem. Immunol. **66:**209–230.
66. **Yano, A., et al.** 2002. Roles of IFN-gamma on stage conversion of an obligate intracellular protozoan parasite, *Toxoplasma gondii*. Int. Rev. Immunol. **21:** 405–421.
67. **Yarovinsky, F., et al.** 2005. TLR11 activation of dendritic cells by a protozoan profilin-like protein. Science **308:**1626–1629.

Editor: J. F. Urban, Jr.